Journal of Electron Spectroscopy and Related Phenomena 200 (2015) 15–21

Contents lists available at ScienceDirect

Journal of Electron Spectroscopy and Related Phenomena

journal homepage: www.elsevier.com/locate/elspec

Efficient and tunable high-order harmonic light sources for photoelectron spectroscopy at surfaces

Cheng-Tien Chiang[a,b], Michael Huth[a], Andreas Trützschler[a,b], Frank O. Schumann[a], Jürgen Kirschner[a,b], Wolf Widdra[b,a,*]

[a] Max-Planck-Institut für Mikrostrukturphysik, Weinberg 2, D-06120 Halle(Saale), Germany
[b] Institute of Physics, Martin-Luther-Universität Halle-Wittenberg, Von-Danckelmann-Platz 3, D-06120 Halle(Saale), Germany

ARTICLE INFO

Article history:
Available online 13 April 2015

Keywords:
High-order harmonic generation
Photoelectron spectroscopy
Ag(0 0 1)

ABSTRACT

With the recent progress in high-order harmonic generation (HHG) using femtosecond lasers, laboratory photoelectron spectroscopy with an ultrafast, widely tunable vacuum-ultraviolet light source has become available. Despite the well-established technique of HHG-based photoemission experiments at kilohertz repetition rates, the efficiency of these setups can be intrinsically limited by the space-charge effects. Here we present recent developments of compact HHG light sources for photoelectron spectroscopy at high repetition rates up to megahertz, and examples for angle-resolved photoemission experiments are demonstrated.

1. Introduction

Photoelectron spectroscopy (PES) has evolved into a powerful method to explore the electronic structure of materials. With the rapidly growing interest in material science with emphasis on the novel electronic properties, further development of modern PES and its light sources is strongly motivated [1,2]. To map the electronic structure in general, photoemission experiments can be performed using polarized light with a widely tunable photon energy range. Conventional light sources are the synchrotron radiation and laboratory discharge lamps. Recently, with the development of high-order harmonic generation (HHG) from gases using femtosecond lasers, HHG-based laboratory PES has allowed characterization of electronic systems on the sub-femtosecond time scale [3–6].

In the earlier development of HHG light sources, the repetition rate of HHG was limited at a few hertz due to the necessary high pulse energy of several mJ using picosecond lasers [19,20]. By using Ti:sapphire femtosecond lasers Linder and Heyl et al. later demonstrated HHG at 100 kHz with μJ laser pulses [21,22]. Details of the development of HHG light sources have been reviewed elsewhere [23–26]. The higher repetition rate of HHG light sources is of crucial importance for photoemission experiments on solids because of the space-charge effects. The space-charge effects result from the Coulomb repulsion between photoelectrons from the same light pulse. They impose a margin on the number of emitted photoelectrons per pulse, beyond which an energy and momentum broadening in photoemission spectra can occur [27]. As we summarize in Fig. 1, conventional HHG-based PES setups mainly work at few kHz, therefore the space-charge effects can limit the photoemission intensity to several thousands photoelectrons per second.

To further increase the efficiency of HHG-based PES, it becomes necessary to extend the repetition rate of HHG light sources into the megahertz range. As already demonstrated in several elegant optical experiments, MHz HHG can be achieved by using high power laser systems working simply at MHz, or by additional enhancements such as a resonant cavity or plasmonic nanostructures [28–33]. In addition to these approaches, we demonstrate HHG at MHz using a more compact setup and drive HHG directly by a Ti:sapphire long cavity oscillator [34] or by a compact Yb-fiber laser system. For PES with HHG excitation, the combination with time-of-flight (ToF) electron spectrometers has been proven to be highly efficient [35,36]. Detailed comparison of the absolute photoemission intensity and efficiency of experiments have been addressed before [36] and in this paper we present examples with tunable photon energy and light polarization as well as discuss the new extensive development.

* Corresponding author at: Institute of Physics, Martin-Luther-Universität Halle-Wittenberg, Von-Danckelmann-Platz 3, D-06120 Halle(Saale), Germany.
Tel.: +49 345 552 5360; fax: +49 345 552 7160.
E-mail address: wolf.widdra@physik.uni-halle.de (W. Widdra).

http://dx.doi.org/10.1016/j.elspec.2015.04.001
0368-2048/

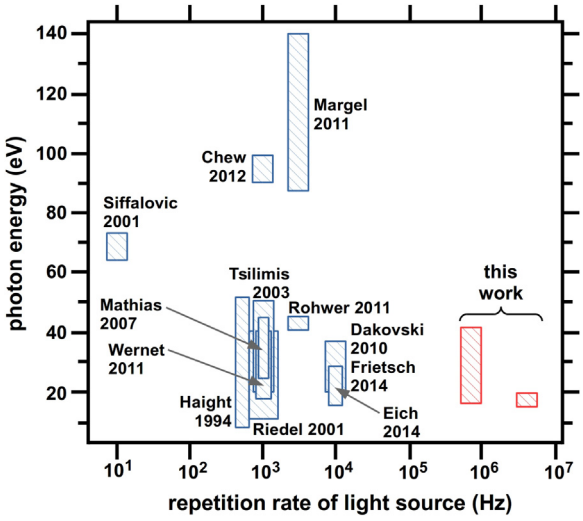

Fig. 1. Overview of HHG-based PES setups highlighted by their photon energy range and repetition rate [7–18]. For clarity, the overlapping kHz [9–12] as well as 10 kHz experiments are shown with different width [16–18].

2. Photoelectron spectroscopy experiments

To demonstrate the tunability of megahertz HHG light sources for laboratory PES, we choose photoemission experiments on a Ag(0 0 1) surface as an example. Photoemission spectra from this surface have been well-documented using synchrotron radiation and the details can be explained by the band structure [40,41]. For photon energies below 23 eV, the harmonics are driven by a Ti:sapphire long cavity laser working at 4 MHz with a photon energy of 1.5 eV, a pulse energy of 650 nJ and a pulse duration of 50 fs [42]. For a wider photon energy range from 18 to 40 eV the harmonics are driven by an Yb-fiber laser system at 0.7 MHz with a photon energy of 1.2 eV, a pulse energy of 14 μJ, and a pulse duration of 300 fs [43]. The output of one of these lasers is focused into an Ar or Xe gas jet in a vacuum chamber and the generated harmonics are selected and focused on the Ag(0 0 1) surface using a commercial monochromator designed for He discharge lamps [44]. The photoelectrons are collected by a time-of-flight (ToF) spectrometer and their energy (E) as well as the two momentum components parallel to the surface (k_x, k_y) are analyzed [35,45]. Details of the HHG and the PES setups have been described in previous publications [36,46,47].

The photoemission spectra measured with *p*- and *s*-polarized harmonics are shown in Fig. 2 for photon energies $h\nu = 17$ and 20 eV driven by the Ti:sapphire laser. From the three-dimensional energy and momentum distribution $I(E, k_x, k_y)$ of photoelectrons down to a binding energy of more than 10 eV, we present in Fig. 2 the two-dimensional slices $I(E, k_x)$ and $I(E, k_y)$. Using the *s*-polarized light at 17 and 20 eV, we observe a different distribution of photoelectrons along the k_x and k_y directions when comparing Fig. 2a with Fig. 2b, as well as Fig. 2c with Fig. 2d. The flat $E - k_x$ dispersion in Fig. 2a and Fig. 2c at the binding energy of around 5 eV is attributed to the Ag *d* band. At comparable binding energies in the $E - k_y$ dispersion in Fig. 2b and Fig. 2d, the *d* band exhibits a slightly downward dispersion. The upward dispersive band at around 2 to 3 eV is assigned to the Ag *sp* band. These assignments are based on the theoretical band structure in Fig. 2g [37] and the observed dispersion can be qualitatively described by the empirical band structure as shown by the circles in Fig. 2b and Fig. 2d [38,39].

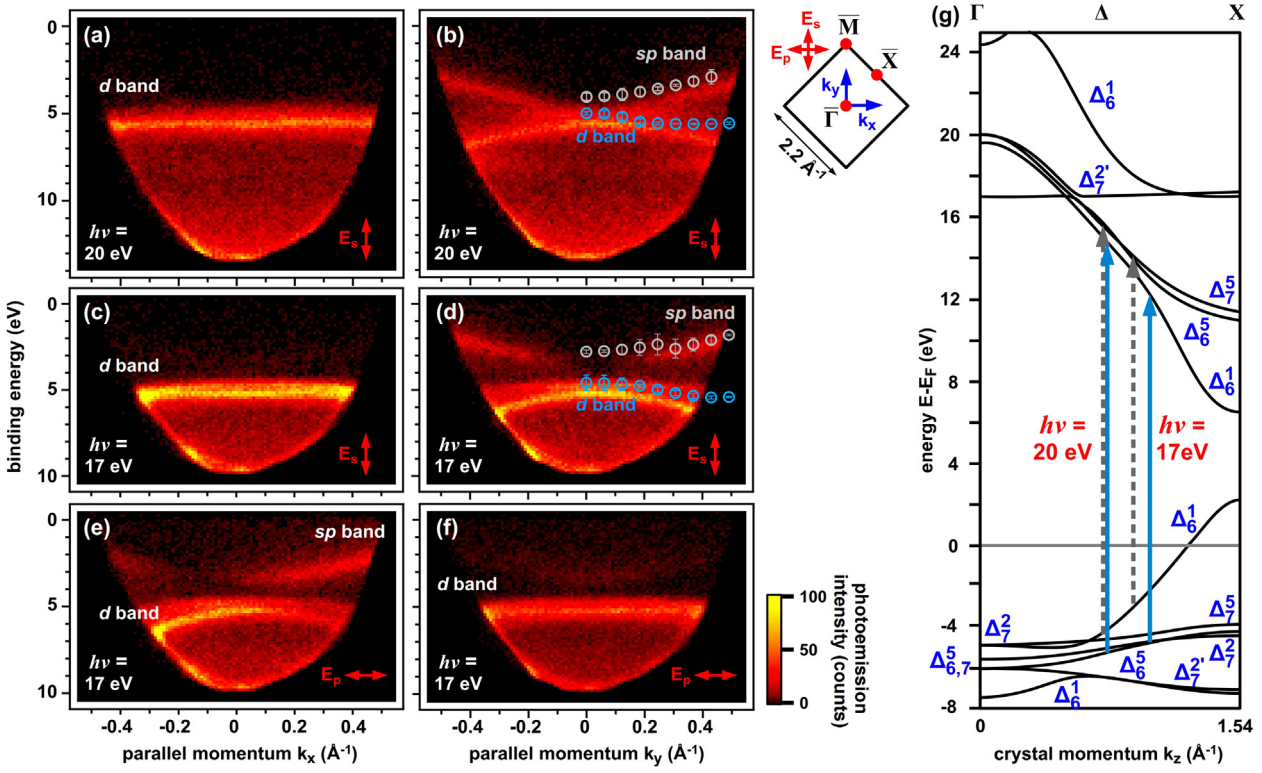

Fig. 2. (a)–(e) Angle-resolved photoemission spectra measured on the Ag(0 0 1) surface along the momentum directions k_x and k_y as indicated by the surface Brillouin zone. The photon energy used is $h\nu = 20$ eV for (a) and (b), and $h\nu = 17$ eV for (c)–(f). The incident light is *s*- and *p*-polarized for (a)–(d) and (e)–(f), respectively. The spectra are integrated over $\Delta k = 0.1$ Å^{-1} perpendicular to the respective momentum direction. The electric field of the *s*-polarization of light is parallel to k_y and the *p*-polarization has a component in the Ag(0 0 1) surface parallel to k_x. The relative orientation between the light polarization and the momentum directions of photoelectrons is shown in the inset with the surface Brillouin zone. Possible transitions for $h\nu = 17$ and 20 eV are indicated in a comparison with theoretical band structure of Ag from Eckardt et al. in (g) [37] and estimated by an empirical band structure at selected momenta [38,39] in (b,d).

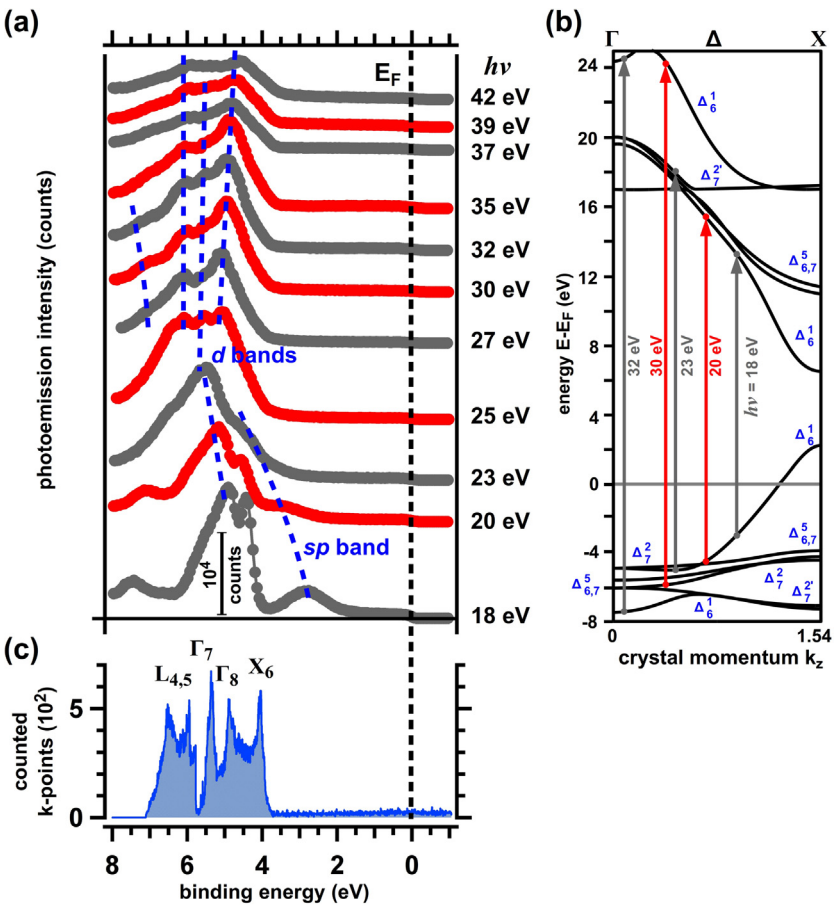

Fig. 3. (a) Photon energy dependent photoemission spectra measured on the Ag(0 0 1) surface. The photoelectrons emitted within ±15° from the surface normal are integrated. For clarity, the spectra are shifted vertically. (b) The theoretical bulk band structure of Ag with possible transitions indicated at various photon energies [37]. (c) Calculated density of states of Ag using empirical band structure [38,48]. Selected high symmetry points are marked.

By going from *s*- to *p*-polarized light at the same photon energy $h\nu = 17$ eV, we observe a significant change in the distribution of photoelectrons as seen in the comparison of Fig. 2c,d and Fig. 2e,f. With *s*-polarized light we observe only the *d* band along the k_x direction (Fig. 2c), and both the *sp* and the *d* bands along the k_y direction (Fig. 2d). In strong contrast, with *p*-polarized light we observe both the *sp* and the *d* bands along the k_x direction (Fig. 2e), but mainly only the *d* band along the k_y direction (Fig. 2f). The observation indicates that photoelectrons with momentum parallel to the polarization of light are emitted in optical transitions from both the *sp* and *d* bands, whereas photoelectrons with momentum perpendicular to the light polarization are mainly emitted in transitions from the *d* band. As the polarization of light is rotated from *s* to *p*, the distribution of photoelectrons is rotated accordingly due to the optical selection rules [49].

The wide tunability in photon energy of HHG-based PES is further demonstrated in Fig. 3a by the angle-integrated photoemission spectra. The photon energy dependence can be qualitatively explained by the band structure in Fig. 3b and by the density of states (DOS) in Fig. 3c [38,48]. At $h\nu = 18$ eV, a resonant transition takes place between the occupied and unoccupied *sp* bands where no significant feature in the DOS appears. As $h\nu$ is increased, transitions can occur between the occupied *d* and unoccupied bands and the dominant photoemission signal from the *d* bands is due to their high DOS at 4–7 eV below the Fermi level. At around $h\nu = 32$ eV, a resonant transition may occur at the bottom of the *sp* band and this is indicated in Fig. 3a at a binding energy of about 7 eV.

3. Further developments

In contrast to the well-established kHz HHG setups for time-resolved PES as summarized in Fig. 1, an efficient and space-charge free MHz HHG setup with reduced complexity can be operated by an individual user for long-term measurements. In this section we introduce the design of a compact generation chamber and a gas-recycling system. The latter is of high importance for long-term experiments due to the costs for rare gases as xenon. In addition, we demonstrate a proof-of-principle long-term operation of the setup. At the end of this section the pulse duration and the bandwidth of the harmonics are discussed.

3.1. Compact generation chamber

The megahertz HHG setup follows a tight-focusing geometry for phase-matching conditions at high backing pressure [26]. In order to suppress mechanical vibrations as well as to be user-friendly, the ideal generation chamber should have a minimal size, which is only limited by the front flange of the vacuum pump with a sufficient pumping speed. Here a turbo pump with a nominal pumping speed of 700 l/s and a front flange with an inner diameter of 150 mm is used [50]. Therefore the generation chamber has about the same inner diameter. In Fig. 4a a photograph of the generation chamber is shown and in Fig. 4b the 30 μm glass capillary [51] for the gas jet can be seen. The laser beam is focused into the gas jet by the lens assembly which consists of an achromatic lens sealing the chamber [52] and a bellow allowing mechanical adjustment. The glass

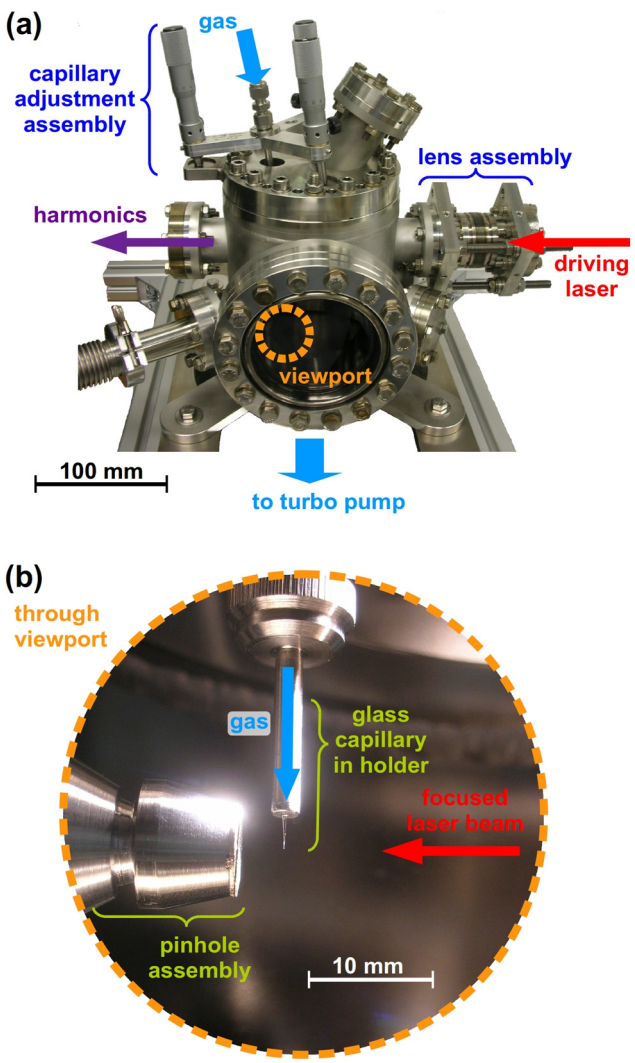

Fig. 4. Photographs of the generation chamber for the harmonics (a), with the glass capillary and the pinhole assembly visible through the viewport as in (b).

capillary in Fig. 4b is mounted in a holder on the top flange of the generation chamber in Fig. 4a. Its position can be adjusted by the tripod via three micrometer screws. Behind the gas jet, a 150 μm pin hole blocks the fundamental driving laser beam and reduces the gas loading in the monochromator chamber thereafter [44].

3.2. Gas-recycling system

The HHG spectrum strongly depends on the generation gas medium [20,23,25]. For higher photon energies gases with higher ionization potential such as He, Ne or Ar are used. On the other hand, HHG from gases with lower ionization potential, *e.g.* Xe and Kr, can lead to several orders of magnitude higher photon flux at lower photon energies. Due to the cost of Xe and Kr in a long-term HHG experiment, it is necessary to recycle the gas from the generation chamber and to compress it to the backing pressure for the gas jet. In Fig. 5a, a simplified gas flow diagram of our recycling system for Xe is presented. The gas jet with a backing pressure of 5 bar is injected into the generation chamber (GC) by the capillary (CA). During the HHG operation, the background pressure of Xe is about 10^{-2} mbar in GC and 1 bar after the scroll pump (SP_1). From the gas reservoir (B_1), the recycled gas can be further compressed by a dry membrane compressor (C) up to 10 bar and stored in an expansion tank (B_2). From there the gas is fed to the pressure regulator (PR) for regulation of the backing pressure of the gas jet. For maintenance the recycling systems can be divided into several parts by the valves ($V_{1,\ldots,10}$) and the gas is stored in B_1 and B_2.

During the operation of the recycling system with Xe, we characterize the recycled gas by a quadrupole mass spectrometer in the experiment chamber (EC) behind the monochromator chamber (MC). In Fig. 5b the black (gray) mass spectrum in the upper panel is measured during (without) the operation of the recycling system about a week after its installation. The gray spectrum shows the residual gas of CO in EC, and the F^+ signal can be attributed to the outgassing of the mass spectrometer itself (electron stimulated desorption). The difference of these two spectra is displayed in the lower panel, showing dominantly the signals of singly and doubly ionized Xe. For comparison the red vertical bars indicate the signals estimated by the relative natural abundance of Xe isotopes [53]. With this gas-recycling system the HHG setup has been operated with the same xenon loading for more than 6 months. For longer operation we observed CO in the residual gas, which could be suppressed by installing an additional adsorption pump in the recycling system.

3.3. Long-term operation

By using the compact generation chamber in combination with the Xe recycling system, we demonstrate the proof-of-principle for a long-term operation of HHG-based photoemission using the Yb-fiber laser. In Fig. 6a,c the count rate of photoelectrons excited by

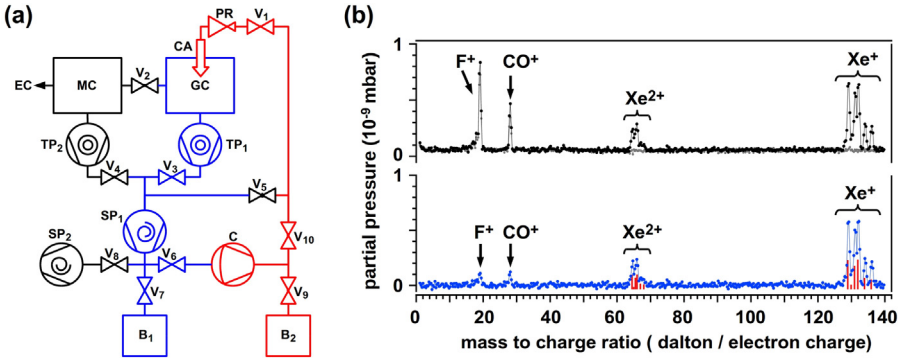

Fig. 5. (a) Simplified flow diagram of the gas-recycling system with high (red) and low (blue) pressure region indicated. GC: generation chamber for the harmonics with gas jet from a glass capillary (CA); MC: monochromator chamber; EC: photoemission experiment chamber; $TP_{1,2}$: turbo pumps; $SP_{1,2}$: scroll pumps; $B_{1,2}$: gas reservoirs; C: compressor; $V_{1,\ldots,10}$: valves; PR: pressure regulator. (b) Mass spectra of residual gas in the photoemission experiment chamber with (black) and without (gray) using Xe in GC. The difference spectrum is shown in the lower panel together with the relative natural abundance of Xe isotopes (red bars) [53]. (For interpretation of the references to color in this figure legend, the reader is referred to the web version of this article.)

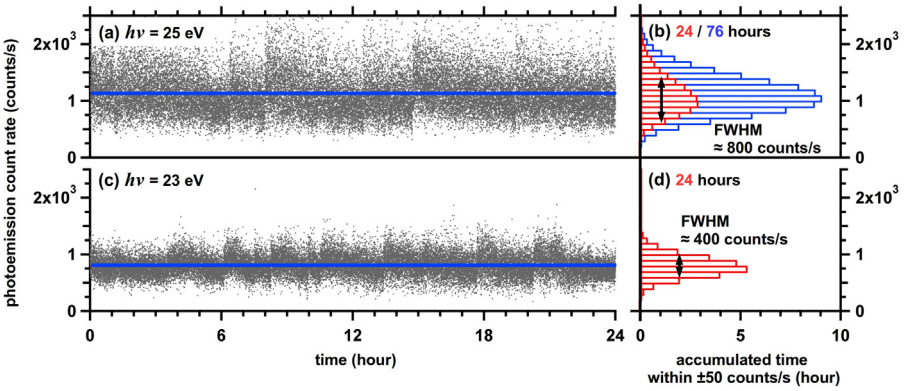

Fig. 6. Photoemission count rate in 24-hour-long measurements with the HHG light source for photon energies (a,b) 25 eV and (c,d) 23 eV. Each data point in (a,c) is measured for about 2.5 s and the average count rate is indicated by the blue horizontal lines at 1100 and 800 counts/s for (a) and (c), respectively. In (b,d) the histograms (red) of the data in (a,c) are shown with their full-width-at-half-maximum (FWHM). In (b) an additional histogram (blue) is taken from a longer measurement for 76 h. (For interpretation of the references to color in this figure legend, the reader is referred to the web version of this article.)

the HHG light source is shown for two independent experiments lasting 24 h. These experiments were performed in conventional laboratory condition without active temperature regulation and the laboratory temperature varied about ±0.5 °C around 22 °C during these days. In order to compensate the influence of the temperature variation on the fiber laser, we actively changed the pulse compressor settings inside the fiber laser and minimized the output pulse duration. In Fig. 6b,d the histograms of the photoelectron count rate in Fig. 6a,c are displayed and the full-width-at-half-maximum (FWHM) is estimated. In addition we show in Fig. 6b a histogram from a longer measurement for 76 h. By comparing the histograms in Fig. 6b we see that the operation of the HHG light source can be extended to several days without additional degradation of its stability.

For a quantitative estimation, we derive the ratio of the FWHM to the average count rate from the histograms in Fig. 6b,d and obtain values of about 0.8 and 0.5 for 25 and 23 eV, respectively. The larger variation for 25 eV could be attributed to its higher harmonic order and a consequently more sensitive generation condition. For comparison, Leitner et al. characterized the shot-to-shot intensity distribution of their HHG setup for a photon energy range from 17 to 27 eV at a repetition rate of 3 kHz, and the FWHM variation amounts to 0.53 of the average intensity [54]. A much smaller FWHM intensity fluctuation of about 0.08 has been demonstrated in a short measurement with 430 shots using a 10 Hz HHG setup at 33 eV for seeding the sFLASH beam line [55]. The stability of our HHG light could be further improved by reducing the temperature variation in the laboratory and by additional damping of the mechanical vibration from the vacuum pumps.

3.4. Bandwidth and pulse duration

Due to the ultimate pulse duration down to a few hundreds of attoseconds, HHG light sources have great potential for time-resolved PES [3,4,6]. To get a train of these short pulses, the harmonics need to be selected and compressed properly after the generation. Moreover, much effort is required in order to single out an isolated sub-femtosecond pulse and to precisely characterize its pulse duration. Details of the available approaches have been reviewed recently [6,57]. Here we estimate the lower limit for the pulse duration of the harmonics according to their bandwidth in photon energy.

The bandwidth of the harmonics can be quantitatively estimated in photoemission experiments. In Fig. 7a we present the width of the Fermi-edge in the photoemission spectra in Fig. 3a. These values (red circles) represent the total energy resolution in the photoemission experiments and they include the energy resolution of the

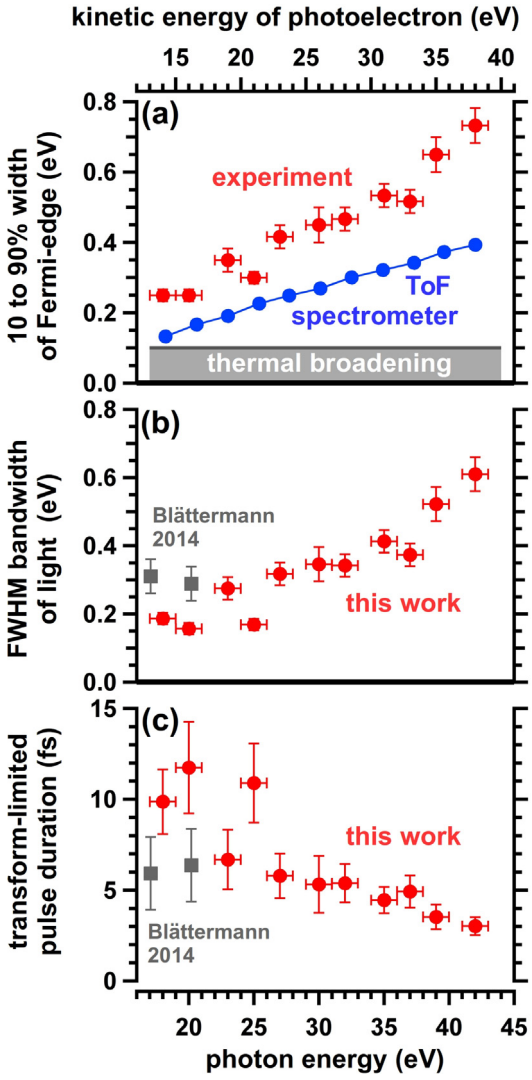

Fig. 7. (a) Red data points are the measured 10–90% width of the Fermi-edge in photoemission spectra in Fig. 2a at the kinetic energies of photoelectrons shown by the top scale and photon energies by the bottom scale. Blue data points are the simulated energy resolution of the ToF spectrometer settings using a conservative estimation of the time resolution of 300 ps for the electronics [47,56]. Gray area indicates the 100 meV thermal broadening at 300 K. (b) Red points show the full-width-at-half-maximum bandwidth of light estimated from data in (a). For comparison, gray squares show the directly measured bandwidth from our previous publication [34]. (c) The transform-limited pulse width (full-width-at-half-maximum, FWHM) estimated from the bandwidth in (b).

ToF electron spectrometer (blue circles), the thermal broadening at 300 K (gray area), as well as the bandwidth of the harmonics. From these data, we estimate the bandwidth of the harmonics in Fig. 7b. In addition, we extract the bandwidth of low energy harmonics driven by the Ti:sapphire laser from a direct measurement published previously (gray squares) [34].

From the bandwidth in Fig. 7b, we estimate the transform-limited pulse duration of a single harmonic pulse in Fig. 7c. The estimated pulse duration ranges from about 3 to 10 fs for photon energies from 40 to 17 eV. In our setup, we use a monochromator grating after the generation in order to select a single harmonic as well as to focus it onto the sample. In this diffraction process, the pulse width is stretched to about 2 ps [58]. However this temporal stretching might be compressed by a second identical grating or other designs [59,60]. In addition to the duration of an single isolated pulse, the duration of the pulse train of the harmonics can be estimated by the pulse duration of the driving lasers, which corresponds to about 50 and 300 fs for Ti:sapphire and Yb-fiber laser, respectively. In order to achieve a better time-resolution, further development to compress either the driving laser or the harmonics is required.

4. Summary

To summarize, light sources based on high-order harmonic generation (HHG) provide a unique opportunity to perform laboratory photoelectron spectroscopy (PES) using linearly polarized light with a wide photon energy range of more than 20 eV. By using the harmonics generated from lasers with megahertz repetition rates ranging from Ti:sapphire oscillators to Yb-based fiber lasers, efficient and space-charge free photoemission experiments are nowadays possible that last for many days without interruption. Here we demonstrate such photon-energy and polarization dependent PES experiments on a Ag(0 0 1) surface. The developments of the compact generation setup, the recycling system for the gases as well as the long-term operation of the HHG light source are presented. In addition, the bandwidth of the harmonics is estimated from the energy broadening in the photoelectron spectra and the lower limit of the pulse duration is given. These modern developments should provide an efficient way for laboratory PES and microscopy as well as for time-resolved experiments in the future.

Acknowledgements

We thank C. Heyl, J. Güdde, K. Duncker, and M. Kiel for fruitful discussions at the initial stage of our experiments, A. Blättermann for the first HHG experiments using the Ti:sapphire laser. An excellent technical support by R. Kulla, S. Helmbach, M. Schröder, R. Neumann, and F. Weiß is gratefully acknowledged. We also thank for financial support from SFB 762.

Appendix A. Supplementary Data

Supplementary data associated with this article can be found, in the online version, at http://dx.doi.org/10.1016/j.elspec.2015.04.001

References

[1] W. Schattke, M. Van Hove (Eds.), Solid State Photoemission and Related Methods, Wiley-VCH, Berlin, 2003.
[2] S. Suga, A. Sekiyama, Photoelectron Spectroscopy: Bulk and Surface Electronic Structures, Springer-Verlag, Berlin Heidelberg, 2014.
[3] A.L. Cavalieri, N. Muller, T. Uphues, V.S. Yakovlev, A. Baltuska, B. Horvath, B. Schmidt, L. Blumel, R. Holzwarth, S. Hendel, M. Drescher, U. Kleineberg, P.M. Echenique, R. Kienberger, F. Krausz, U. Heinzmann, Nature 449 (2007) 1029–1032.
[4] F. Krausz, M. Ivanov, Rev. Mod. Phys. 81 (2009) 163–234.
[5] T. Haarlammert, H. Zacharias, Curr. Opin. Solid State Mater. Sci. 13 (2009) 13–27.
[6] L. Plaja, R. Torres, A. Zaïr (Eds.), Attosecond Physics: Attosecond Measurements and Control of Physical Systems, Springer-Verlag, Berlin Heidelberg, 2013.
[7] P. Siffalovic, M. Drescher, M. Spieweck, T. Wiesenthal, Y.C. Lim, R. Weidner, A. Elizarov, U. Heinzmann, Rev. Sci. Instrum. 72 (2001) 30–35.
[8] R. Haight, D.R. Peale, Rev. Sci. Instrum. 65 (1994) 1853–1857.
[9] D. Riedel, J.L. Hernandez-Pozos, R.E. Palmer, S. Baggott, K.W. Kolasinski, J.S. Foord, Rev. Sci. Instrum. 72 (2001) 1977–1983.
[10] G. Tsilimis, J. Kutzner, H. Zacharias, Surf. Sci. 528 (2003) 171–176.
[11] S. Mathias, L. Miaja-Avila, M.M. Murnane, H. Kapteyn, M. Aeschlimann, M. Bauer, Rev. Sci. Instrum. 78 (2007) 083105.
[12] P. Wernet, J. Gaudin, K. Godehusen, O. Schwarzkopf, W. Eberhardt, Rev. Sci. Instrum. 82 (2011) 063114.
[13] S.H. Chew, F. Süßmann, C. Späth, A. Wirth, J. Schmidt, S. Zherebtsov, A. Guggenmos, A. Oelsner, N. Weber, J. Kapaldo, A. Gliserin, M.I. Stockman, M.F. Kling, U. Kleineberg, Appl. Phys. Lett. 100 (2012) 051904.
[14] E. Magerl, S. Neppl, A.L. Cavalieri, E.M. Bothschafter, M. Stanislawski, T. Uphues, M. Hofstetter, U. Kleineberg, J.V. Barth, D. Menzel, F. Krausz, R. Ernstorfer, R. Kienberger, P. Feulner, Rev. Sci. Instrum. 82 (2011) 063104.
[15] T. Rohwer, S. Hellmann, M. Wiesenmayer, C. Sohrt, A. Stange, B. Slomski, A. Carr, Y. Liu, L.M. Avila, M. Kallane, S. Mathias, L. Kipp, K. Rossnagel, M. Bauer, Nature 471 (2011) 490–493.
[16] G.L. Dakovski, Y. Li, T. Durakiewicz, G. Rodriguez, Rev. Sci. Instrum. 81 (2010) 073108.
[17] B. Frietsch, R. Carley, K. Döbrich, C. Gahl, M. Teichmann, O. Schwarzkopf, P. Wernet, M. Weinelt, Rev. Sci. Instrum. 84 (2013) 075106.
[18] S. Eich, A. Stange, A. Carr, J. Urbancic, T. Popmintchev, M. Wiesenmayer, K. Jansen, A. Ruffing, S. Jakobs, T. Rohwer, S. Hellmann, C. Chen, P. Matyba, L. Kipp, K. Rossnagel, M. Bauer, M. Murnane, H. Kapteyn, S. Mathias, M. Aeschlimann, J. Electron Spectrosc. Relat. Phenomena 195 (2014) 231–236.
[19] A. McPherson, G. Gibson, H. Jara, U. Johann, T.S. Luk, I.A. McIntyre, K. Boyer, C.K. Rhodes, J. Opt. Soc. Am. B 4 (1987) 595.
[20] M. Ferray, A. L'Huillier, X.F. Li, L.A. Lompre, G. Mainfray, C. Manus, J. Phys. B: Atomic Mol. Opt. Phys. 21 (1988) L31.
[21] F. Lindner, W. Stremme, M. Schätzel, F. Grasbon, G. Paulus, H. Walther, R. Hartmann, L. Strüder, Phys. Rev. A 68 (2003) 013814.
[22] C. Heyl, J. Güdde, U. Höfer, A. L'Huillier, Phys. Rev. Lett. 107 (2011) 033903.
[23] C. Winterfeldt, C. Spielmann, G. Gerber, Rev. Mod. Phys. 80 (2008) 117–140.
[24] T. Brabec (Ed.), Strong Field Laser Physics, Springer-Verlag, Berlin Heidelberg, 2009.
[25] T. Popmintchev, M.-C. Chen, P. Arpin, M.M. Murnane, H.C. Kapteyn, Nat. Photon 4 (2010) 822–832.
[26] C.M. Heyl, J. Güdde, A. L'Huillier, U. Höfer, J. Phys. B: Atomic Mol. Opt. Phys. 45 (2012) 074020.
[27] S. Hellmann, K. Rossnagel, M. Marczynski-Bühlow, L. Kipp, Phys. Rev. B 79 (2009) 035402.
[28] S. Hädrich, A. Klenke, J. Rothhardt, M. Krebs, A. Hoffmann, O. Pronin, V. Pervak, J. Limpert, A. Tünnermann, Nat. Photon 8 (2014) 779–783.
[29] C. Benko, T.K. Allison, A. Cingoz, L. Hua, F. Labaye, D.C. Yost, J. Ye, Nat. Photon 8 (2013) 530–536.
[30] I. Pupeza, S. Holzberger, T. Eidam, H. Carstens, D. Esser, J. Weitenberg, P. Ruszbuldt, J. Rauschenberger, J. Limpert, T. Udem, A. Tünnermann, T.W. Hänsch, A. Apolonski, F. Krausz, E. Fill, Nat. Photon 7 (2013) 608–612.
[31] M. Sivis, M. Duwe, B. Abel, C. Ropers, Nature 485 (2012) E1–E3.
[32] M.B. Raschke, Annalen der Physik 525 (2013) A40–A42.
[33] N. Pfullmann, M. Noack, J. Cardoso de Andrade, S. Rausch, T. Nagy, C. Reinhardt, V. Knittel, R. Bratschitsch, A. Leitenstorfer, D. Akemeier, A. Htten, M. Kovacev, U. Morgner, Annalen der Physik 526 (2014) 119–134.
[34] A. Blättermann, C.-T. Chiang, W. Widdra, Phys. Rev. A 89 (2014) 043404.
[35] M.H. Berntsen, O. Gotberg, O. Tjernberg, Rev. Sci. Instrum. 82 (2011) 095113.
[36] C.-T. Chiang, M. Huth, A. Trützschler, M. Kiel, F.O. Schumann, J. Kirschner, W. Widdra, N. J. Phys. 17 (2015) 013035.
[37] H. Eckardt, L. Fritsche, J. Noffke, J. Phys. F: Met. Phys. 14 (1984) 97.
[38] R. Benbow, N. Smith, Phys. Rev. B 27 (1983) 3144–3151.
[39] In the two-dimensional cut ΓXWKWX of the fcc bulk Brillouin zone, the energy bands of Ag are calculated at 507 points using the empirical Hamitonian in Ref. [38], 2014.
[40] U. König, P. Weinberger, J. Redinger, H. Erschbaumer, A.J. Freeman, Phys. Rev. B 39 (1989) 7492–7499.
[41] S.C. Wu, C.K.C. Lok, J. Sokolov, J. Quinn, Y.S. Li, D. Tian, F. Jona, J. Phys.: Condens. Matter 1 (1989) 4795.
[42] Femtosource scientific XL 650, 2011. Femtolasers Produktions GmbH, Vienna, Austria.
[43] Impulse, ytterbium-fiber laser system, 2013. Clark-MXR, Inc., Dexter, USA.
[44] MBS M-1 VUV monochromator, 2012. 1200 lines/mm, MB Scientific AB, Uppsala, Sweden.
[45] Themis 1000, 2010. SPECS Surface Nano Analysis GmbH, Berlin, Germany.
[46] C.-T. Chiang, A. Blättermann, M. Huth, J. Kirschner, W. Widdra, Appl. Phys. Lett. 101 (2012) 071116.
[47] M. Huth, C.-T. Chiang, A. Trützschler, F.O. Schumann, J. Kirschner, W. Widdra, Appl. Phys. Lett. 104 (2014) 061602.

[48] In the irreducible 1/48 part of the Brillouin zone (BZ), the 42 energy bands of Ag are calculated at 11760 points using the Hamitonian in Ref. [38]. The DOS is estimated by a histogram with a 10 meV width of bins, and its apparent dip near 6 eV may be due to the limited sampling points in the BZ, 2014.
[49] W. Eberhardt, F.J. Himpsel, Phys. Rev. B 21 (1980) 5572–5576.
[50] HiPace 700, 2011. Pfeiffer Vacuum GmbH, Asslar, Germany.
[51] Micropipette made from borosilicate glass, 2013. Hilgenberg GmbH, Malsfeld, Germany.
[52] Achromatic doublet, AC254-050-B, 2013. Thorlabs Inc., Newton, USA.
[53] J.E. Sansonetti, W.C. Martin, J. Phys. Chem. Ref. Data 34 (2005) 1559–2259.
[54] T. Leitner, A.A. Sorokin, J. Gaudin, H. Kaser, U. Kroth, K. Tiedtke, M. Richter, P. Wernet, N. J. Phys. 13 (2011) 093003.
[55] T. Maltezopoulos, M. Mittenzwey, A. Azima, J. Bödewadt, H. Dachraoui, M. Rehders, C. Lechner, M. Schulz, M. Wieland, T. Laarmann, J. Roßbach, M. Drescher, Appl. Phys. B 115 (2014) 45–54.
[56] Charged particle trajectory simulation program SIMION, 2012. Scientific Instrument Services, Inc., Ringoes, USA.
[57] M. Chini, K. Zhao, Z. Chang, Nat. Photon 8 (2014) 178–186.
[58] M. Bauer, J. Phys. D: Appl. Phys. 38 (2005) R253.
[59] H. Igarashi, A. Makida, M. Ito, T. Sekikawa, Opt. Express 20 (2012) 3725–3732.
[60] L. Poletto, P. Miotti, F. Frassetto, C. Spezzani, C. Grazioli, M. Coreno, B. Ressel, D. Gauthier, R. Ivanov, A. Ciavardini, M. de Simone, S. Stagira, G.D. Ninno, Appl. Opt. 53 (2014) 5879–5888.